Magnetic neutron spectroscopy of a spin-transition Mn^{3+} molecular complex

Karl Ridier, Sylvain Petit, Béatrice Gillon, and Grégory Chaboussant*
Laboratoire Léon Brillouin, UMR12, Commissariat l'Énergie Atomique et aux Énergies Alternatives, Centre National de la Recherche Scientifique, F-91191 Gif-sur-Yvette, France

Damir A. Safin and Yann Garcia
Institute of Condensed Matter and Nanosciences, Molecules, Solids, and Reactivity, Université Catholique de Louvain, Place Louis Pasteur 1, 1348 Louvain-la-Neuve, Belgium

(Received 6 June 2014; revised manuscript received 7 August 2014; published 8 September 2014)

We have investigated by inelastic neutron scattering (INS), neutron diffraction, and magnetometry the magnetic properties of the mononuclear complex $[Mn^{3+}(pyrol)_3(tren)]$ in both high-spin (^5E, HS, $S = 2$) and low-spin ($^3T_1$, LS, $S = 1$) states. The system presents a spin transition (ST) around 47 K with a small hysteresis width ($T_{ST,\uparrow} = 47.5$ K and $T_{ST,\downarrow} = 46$ K) characteristic of an efficient collective transition process. In the HS state, the INS spectrum at 56 K and zero magnetic field is accounted for by a zero-field splitting with $D = -5.73(3)$ cm^{-1} and $|E| = +0.47(2)$ cm^{-1} which may be the result of a dynamic Jahn-Teller effect reported in the literature. In the LS state, a single magnetic peak at 4.87 meV is observed, still at zero field. Despite the existence of an unquenched orbital moment ($L = 1$) in the ground $^3T_1$ state, we argue that it may be described by a genuine $S = 1$ spin Hamiltonian owing to the existence of a strong trigonal distortion of the Mn^{3+} coordination octahedron. The observed peak corresponds to a transition $\Delta M = +1$ within the $S = 1$ ground state split by a large single-ion anisotropy term $D = +39.3$ cm^{-1}. A full spin-Hamiltonian model is proposed based on these first INS results obtained in a thermal ST molecular magnetic system.

DOI: 10.1103/PhysRevB.90.104407 PACS number(s): 75.10.Dg, 75.30.Wx, 75.50.Xx, 78.70.Nx

I. INTRODUCTION

In molecular clusters containing transition-metal ions with $3d^n$ ($n = 4$–7) configuration in quasioctahedral coordination, the application of an external stimulus (temperature, light, pressure, or magnetic field) may trigger a so-called spin transition (ST) between a low-spin (LS) and a high-spin (HS) state. If the right conditions (abruptness, presence of hysteresis, suitable temperature range) are met, this effect could be exploited for applications in the spintronics devices, molecular switches, and sensors [1]. Indeed, along with the magnetic ground-state change, the ST is often accompanied by a change of volume through bond lengths variation, which has important effects in the optical, dielectric, structural, and even mechanical properties [2,3]. Spin transition is usually observed in octahedrally coordinated molecular complexes of Co^{2+}, Fe^{2+}, Fe^{3+}, and, more rarely, d^4 ions like Mn^{3+} and Cr^{2+}, but also in some perovskites like $CsMnF_4$ [4]. The ST in $3d$ ions is governed by the competition between (a) the ligand field which splits the $3d$ levels into a lower t_{2g} triplet and an upper e_g doublet, enforcing electron pairing, and (b) the electronic intra-atomic Coulomb repulsion which promotes a HS ground state. Beyond this competition, the spin transition may also be influenced by a subtle interplay between intermolecular effects [5] and local distortions of the coordination sphere induced by ST. This coupling determines to a large part the level of cooperativity and therefore the dynamics of the ST itself. A dominant cooperative process may lead to significant hysteresis in the ST temperatures. In $3d^4$ ions the spin crossover takes place between $^3T_1$ (LS, $S = 1$) and ^5E (HS, $S = 2$) states. In both states, spin-orbit (SO) coupling (first order in the LS state, second order in the HS state) may result in deviation of the susceptibility from a Curie law implied by effective zero-field splitting (ZFS) terms that can be unequivocally determined only by spectroscopic techniques like neutron scattering or high-field Electron Paramagnetic Resonance (EPR).

In this article, we report by zero-field inelastic neutron scattering (INS) a full insight of the magnetic ground states, in *both* HS and LS states, of $[Mn^{3+}(pyrol)_3(tren)]$. More precisely, the HS and LS states' anisotropy parameters are determined *at zero field* and their relationships with local structural distortions away from purely octahedral geometry are discussed. This compound is the first example of an abrupt ST ($T_{ST} \approx 47$ K) in a $3d^4$, signaling a highly cooperative transition [6–10]. Indeed, if we exclude one example [11], most Mn^{3+} complexes exhibit smooth ST [12–15]. It appears that the driving force for ST in the present case may be different from that of most compounds. First, we note that there are no noticeable intermolecular exchange pathways between the Mn^{3+} ions. The large average Mn-Mn separation ($d \approx 7.40$ Å in both states) leads quite rationally to the provisory conclusion that there is no intermolecular magnetic exchange. Furthermore, Raman spectroscopy and dielectric constant measurement studies [8,16] suggest that the conventional ST process (collective vibrational process) is not operative here but is essentially due to some structural disorder in the HS state associated with a strong high-frequency dynamic Jahn-Teller (JT) effect. This scenario is also supported by high-field EPR data [17,18] and high-field optical spectroscopy [19].

In this context, we have taken advantage of magnetic neutron spectroscopy to address the relationships between the zero-field split ground states (both in LS and HS states) and the local structural distortions. We find that the HS state is indeed anisotropic, with a negative axial term, reflecting the

*gregory.chaboussant@cea.fr

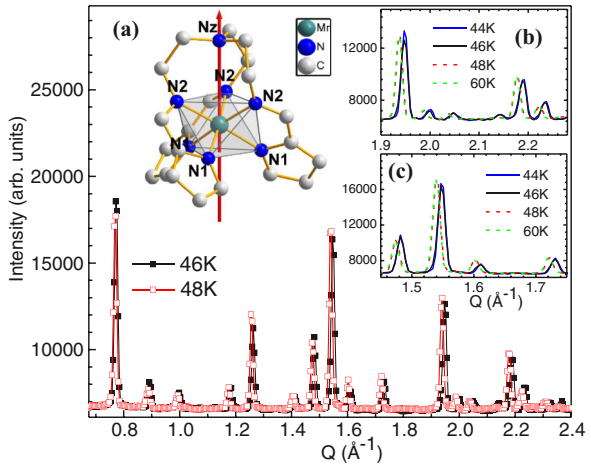

FIG. 1. (Color online) (a) Full Q-range powder neutron diffraction ($\lambda = 2.4226$ Å, G 4.1, LLB-Orphée, Saclay) across the ST at 46 and 48 K and representation of the molecular unit. N atoms are labeled N_z, N_1, and N_2 depending on their coordination type. The red arrow represents the threefold axis of the molecule which also corresponds to a remarkable compression direction of the coordination octahedron. Diffraction data were carried out while warming up from base temperature. (b) and (c) Diffraction patterns at 44, 46, 48, and 60 K on two selected Q ranges ($Q = 1.75$ and 2.1 Å^{-1}). The sudden shift around 47 K is a typical feature of the HS to LS transition.

spatial and temporal averaging of the JT trigonal distortions, and that the LS state is characterized by a strong positive axial anisotropy driven by an important trigonal compression.

II. EXPERIMENTS

$[Mn^{3+}(pyrol)_3(tren)]$ was prepared adapting a procedure for the Fe^{3+} analog [20]. It represents a mononuclear chelate complex where $(pyrol)_3(tren)$ is a tripodal anion containing a Schiff base. The structure has been determined by x-ray diffraction in both HS and LS states by Guionneau *et al.* [9]. It crystallizes in the cubic space group $I\bar{4}3d$ and no structural transition is observed in the whole temperature range. The unit-cell contraction between 293 and 30 K is about 4.7% (2% can be attributed to ST and about 2.7% can be attributed to the thermal contraction). The Mn ion lies on a threefold C_3 "z" axis alongside the uncoordinated N_z(tren) and is octahedrally surrounded by six N atoms (Fig. 1). The coordinating N atoms come from three pyrrole groups at 2.05 Å (denoted N_1) and three imine groups at 2.12 Å (denoted N_2). Nearest-neighbor Mn $\cdots$ N distances are, on average, shorter in the LS state (30 K) than in the HS state (60 K) by about 0.1 Å .

Diffraction data also show the existence of a strong trigonal compression of the Mn^{3+} coordination environment, in both phases, along the C_3 axis (compression of about 10% between the two triangular planes of the N atoms in N_1 and N_2 positions compared to a regular octahedron). As the trigonal ligand field does not lift the degeneracy of the e_g orbital, the HS state is accompanied by strong dynamic JT distortions along the three N_1-Mn-N_2 axes. Diffraction data consist then of the averaged sum of these configurations. On the other hand, the LS state is a so-called JT inactive state due to the unoccupied e_g orbital [10] so that its distortion appears to be static.

Superconducting quantum interference device measurements were performed on a fine powder ($m = 20.1$ mg) placed in a cellulose capsule. The susceptibility measurements were recorded under 500 G in the range 2–300 K (ramp up and down) and corrected for diamagnetic corrections while the magnetization was recorded at various temperatures in the range 0–7 T. Powder neutron diffraction was performed on the G4.1 diffractometer (LLB-Orphée, $\lambda = 2.4226$ Å) between 1.7 and 60 K. The undeuterated sample was placed in a cylindrical Vanadium sample holder. Inelastic scattering experiments were performed on the 4F2 triple-axis spectrometer at LLB-Orphée with a vertical field cryomagnet (0–9 T). The sample was placed in an aluminium container of 10 mm in diameter and 30 mm in height. The powder was pressed by aluminium blocks. The hydrogen in the molecules generates a relatively high incoherent flat background but also induces significant phonon scattering. In the course of the experiment we have used two configurations: $k_f = 1.2$ Å^{-1} (high-resolution low-energy elastic line full width at half maximum (FWHM) equals 0.1 meV) and $k_f = 1.55$ Å^{-1} (high-energy low-resolution elastic line FWHM equals 0.2 meV). INS experiments were done for the most part either at 5 K (LS $S = 1$ state) or at 56 K (HS $S = 2$ state). The transition around 47 K was followed closely during warming.

III. RESULTS AND DISCUSSION

As shown in Fig. 1, we observe the sudden change of the powder neutron-diffraction pattern between 46 and 48 K. The sudden shift of Bragg peaks toward low-Q's upon warming indicates an increase of the lattice parameters and clearly signals the occurrence of an abrupt ST from the LS to the HS state. This shift and the fact that no line broadening could be observed show that the transition is quasicomplete (at least within the accuracy of neutron diffraction) and compatible with a highly cooperative process. Figure 2 shows the magnetic susceptibility, represented as χT on cooling and heating. At high temperature, χT reaches a plateau at 3.06 cm^3 K/mol, in good agreement with the value $\chi T = 4N\mu_B^2 S(S+1)/3k_B = 3$ cm^3 K/mol expected for a Mn^{3+} $S = 2$ HS state without orbital angular momentum [21]. At $T \approx 47 \pm 1$ K we observe the abrupt ST toward the $S = 1$ LS state and a rapid drop off to zero due to first-order SO coupling [22]. Upon slow cooling or heating (0.1 K/min), the χT curve is characterized by a small hysteresis width (see the inset panel in Fig. 2) with $T_{ST,\uparrow} = 47.5$ K and $T_{ST,\downarrow} = 46$ K in agreement with previously published data [6–8]. Note that experiments under high magnetic field (up to ~23 T) evidenced a slight decrease of the transition temperature (~1.5 K) [7]. A first attempt modeling χT in the LS state (0–45 K) with a $S = 1$ Hamiltonian including a single-ion anisotropy term DS_z^2 and a Zeeman term gives the following parameters: $D \approx 44$ cm^{-1} (5.4 meV) and $g = 2.30$. As discussed later in the text, the D value will be adjusted based on the INS data (represented as the dotted line in Fig. 2). In the HS state, the susceptibility is almost constant down to T_{ST} and it is thus hardly possible to extract all the microscopic parameters (D, E, Landé factors) with confidence. The small downturn

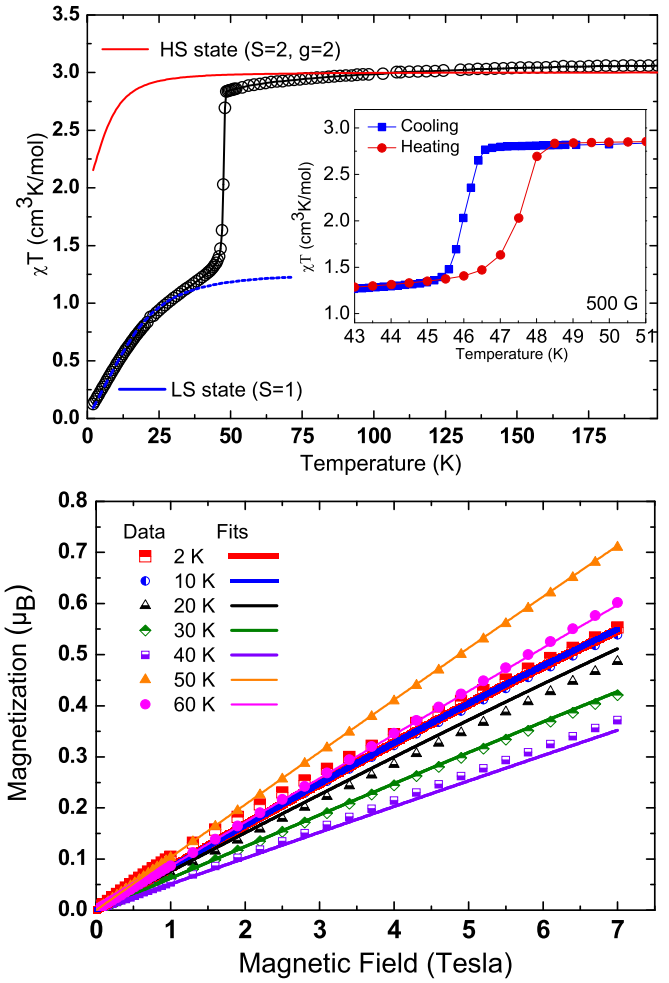

FIG. 2. (Color online) Top panel: Susceptibility curve represented as χT as a function of temperature obtained at 0.05 T during cooling and warming. Inset: Small hysteresis observed around the transition at $T \approx 47$ K. Bottom panel: Magnetization curves at different temperatures (2–60 K). In the LS state ($T \leqslant 45$ K), $\chi T(T)$ and $M(H)$ have been fitted simultaneously (solid lines) using Eq. (1) with $S = 1$ and $g_{\parallel} = 2.12$, $g_{\perp} = 2.30$, $D = 39.3$ cm^{-1}, and $E = 0$, D being fixed from the INS data (*vide infra*). In the HS state ($T \geqslant 50$ K), the red line in the top panel is an attempt made to reproduce the susceptibility using Eq. (1) with $S = 2$ and $g_x = g_y = g_z = 2.00$, $D = -5.73$ cm^{-1}, and $|E| = 0.475$ cm^{-1}, D and E being also fixed from the INS data. The magnetization curves (50 and 60 K) are reproduced using a Brillouin function with $S = 2$ and $g = 1.96$.

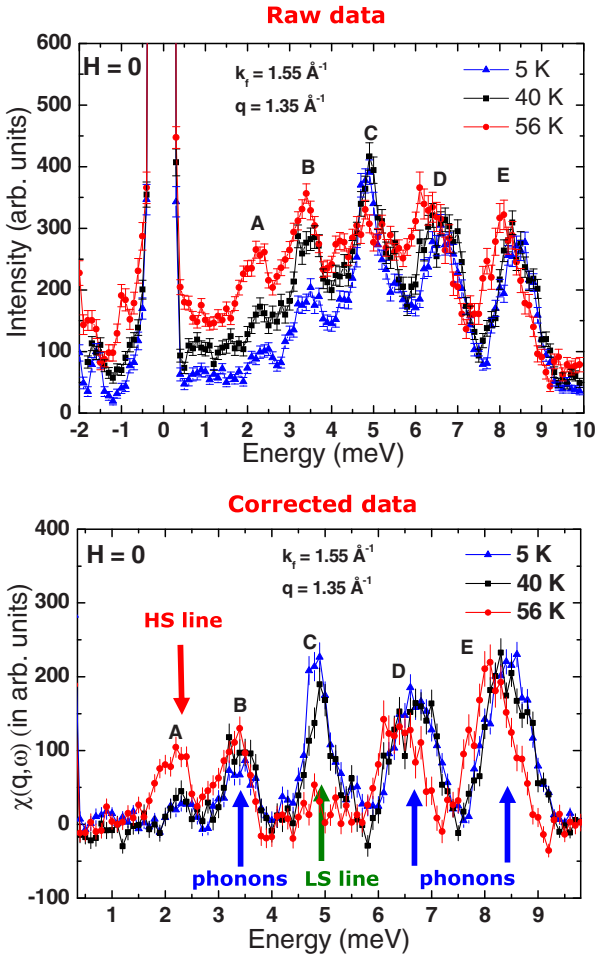

FIG. 3. (Color online) Top panel: INS spectra of [Mn^{3+}(pyrol)$_3$(tren)] ($k_f = 1.55$ Å^{-1}, 4F2, LLB-Orphée, Saclay) obtained at 5, 40, and 56 K and $q = 1.35$ Å^{-1}. The INS transitions are labeled A to E as discussed in the text. Bottom panel: Same set of data but corrected for incoherent background and the population factor $n(\omega,T)$ to account for the contribution due to the phonons' density of states (DOS) $G(\omega)$: $I_{\text{phonons}}(\omega,T) \approx G(\omega)[1 + n(\omega,T)]$.

behavior of χT between 50 and 100 K could be attributed to anisotropic Landé factors and/or pretransitional effects where few individual molecules start to alternate back and forth between HS and LS, thereby lowering the resulting magnetic moment, but no collective transition occurs yet (see Her *et al.* [23] in support of this scenario). In Fig. 2 we show an attempt to reproduce the susceptibility in the HS state using Eq. (1) with $S = 2$ and $g = g_{i=x,y,z} = 2.00$, $D = -5.73$cm^{-1}, and $|E| = 0.475$ cm^{-1} (D and E have been determined from INS data as discussed later). The Landé factors have been set to $g = 2.00$ from powder high-field EPR [17] but small deviations (anisotropic g values) are bound to improve the agreement. This procedure, however, will lead to a clear case of overparametrization due to the very limited variation of χT in the temperature range of relevance ($T \geqslant T_{\text{ST}}$). The magnetization curves in the range 0–7 T are shown in the bottom panel of Fig. 2. While the magnetization curves in the HS state (50 and 60 K) follow a Brillouin function with $S = 2$ and $g = 1.96$ (close to the expectation value), the situation is different in the LS state. $M(H)$ is linear, even at 2 K, in the entire magnetic-field range and reaches only $0.55\mu_B$/molecule at 7 T, very far from the expected saturated magnetization for $S = 1$ ($2\mu_B$/molecule). This typically signals the existence of strong SO coupling and therefore magnetic anisotropy. Best fits to the LS state data are presented in Fig. 2 using a model inferred from the INS data discussed below.

The overall temperature dependence of the zero-field INS spectra is shown in Fig. 3. There are five identified peaks labeled A–E. We argue that the prominent peak C at 4.9 meV is the only visible INS magnetic transition in the LS state, while peak A is the only visible INS magnetic transition in the HS state in the range 1–10 meV. This is asserted by the temperature dependence after correction of the phonon density

of state (Bose correction output shown in the bottom panel of Fig. 3). Only peaks A and C depend on the spin state of the Mn^{3+} ion, suggesting that peaks B, D, and E are most likely due to phonon modes. Indeed, the large and broad peaks D and E, at 6.7 and 8.5 meV, respectively, are field independent and they experience a measurable shift (≈3–3.5%) due to changes in Mn–N bond lengths and cell parameters across ST. This is an expected feature of HS-LS transitions where longer bond lengths lead naturally to a decrease of the phonon mode energies. This has been suggested by density functional theory calculation of the Raman spectra in Fe^{2+} monomers [24]. The HS state, which can only be observed at high temperature, is more difficult to address in this configuration as most of the action takes place below 3 meV. Only one broad peak, labeled A, is visible, at 2.1–2.3 meV. To address more precisely this peak and eventual peaks at lower energies, we used a higher-resolution setting (Fig. 4).

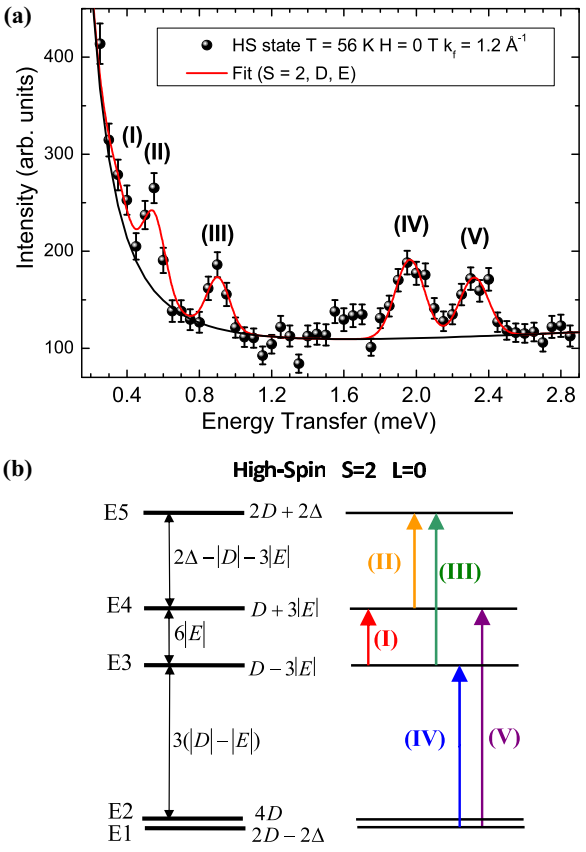

FIG. 4. (Color online) (a) INS spectra of $[Mn^{3+}(pyrol)_3(tren)]$ obtained in the HS state ($S = 2$) at 56 K. Best fits to the data are represented as solid lines with flat background $y_0 = 90$ and a Lorentzian elastic line shape centered at $E = 0$. The resulting background is represented by the black solid line. (b) Energy diagram derived from the zero-field spin Hamiltonian $H = DS_z^2 + E(S_x^2 - S_y^2)$ with $S = 2$ and $D < 0$. The best agreement is obtained for $D = -0.711$ meV and $|E| = +0.059$ meV. Energy levels are $E_1 = 2D - 2\Delta$ (an almost pure $M = \pm 2$ state for small rhombicity E and lowest in energy for $D < 0$), $E_2 = 4D$ ("$M = \pm 2$" as well), $E_3 = D - 3E$ ($M = \pm 1$), $E_4 = D + 3E$ ($M = \pm 1$), and $E_5 = 2D + 2\Delta$ ("$M = 0$"). In these expressions we have $\Delta = (D^2 + 3E^2)^{1/2}$. The five observed transitions are shown in the far right panel. The peak linewidths are FWHM ≈ 0.13 meV for peaks I–III and FWHM ≈ 0.18 meV for peaks IV and V.

TABLE I. High-spin $S = 2$ INS transitions and fit parameters (energy and amplitude of the transitions) compared to calculations using a $S = 2$ spin Hamiltonian [Eq. (1)]. INS peaks were fitted simultaneously using Gaussian line shapes. Transition INS intensities were calculated using MAGPACK [25] with $D = -0.711(4)$ meV and $|E| = +0.059(2)$ meV. The last column shows the ratio between experiment and calculation after normalization using transition IV as a reference.

Transition	E (meV)	A_{exp}	A_{calc}	A_{calc}/A_{exp} (norm.)
I	0.355	40	0.115	1.26
II	0.548	112	0.348	1.16
III	0.903	75	0.317	0.85
IV	1.960	108	0.391	1.00
V	2.315	81	0.305	0.96

A. High-spin state $T \geqslant 48$ K

Figure 4 shows the spectrum at 56 K and $k_f = 1.2$ Å^{-1}, after integration of $q = 1.1$- and 1.35-Å^{-1} data (we checked that—as expected for isolated monomers—the INS transitions are constant in energy as a function of q). Four transitions can clearly be observed between 0.5 and 2.5 meV, labeled II to V. The solid line is a global fit, with the energy and intensity parameters reported in Table I. The background function consists of an elastic line and a flat background. The peak widths are FWHM ≈ 0.13 meV (for peaks I–III) and FWHM ≈ 0.18 meV (for peaks IV and V), in accordance with a loss in resolution with increasing energy transfer. The peak at 0.37 meV, labeled I, is merged into the elastic line and is therefore difficult to simulate, but it is fully accounted for in our simulations.

In our model, the HS ^5E ($L = 0, S = 2$) ground state is described using a spin-only Hamiltonian since no first-order orbital moment is operative:

$$\hat{H} = \hat{H}_{ZFS} + \hat{H}_{Ze} = D\hat{S}_z^2 + E\left(\hat{S}_x^2 - \hat{S}_y^2\right) + \bar{\bar{g}}\mu_B \vec{S} \cdot \vec{B}, \quad (1)$$

where D and E are the axial and rhombic terms of the zero-field splitting (ZFS) and $\bar{\bar{g}}$ is the Landé factor. The corresponding energy levels for $S = 2$ and $D < 0$ are schematically displayed in Fig. 4(b). The nondiagonal E term introduces quantum state mixing between spin states of quantum number M separated by ±2 ($\Delta M = \pm 2$). Then, $M = \pm 2$ states can mix with $M = 0$, but not with $M = \pm 1$, which only mix together (entangled). E_2 and E_1 are very close in energy and will be considered as degenerate in our analysis so that peaks IV and V are actually each composed of two unresolved peaks. E_3 and E_4 are separated by $6|E|$, independently of D. Table I summarizes the main results: the INS transitions ($\Delta M = 0, \pm 1$) are all labeled and identified within the model of Eq. (1). Best fits to the five INS peaks lead to $D = -0.711 \pm 0.004$ meV and $|E| = 0.059 \pm 0.002$ meV [solid line in Fig. 4(a)]. Energy positions and intensities are accounted for with excellent overall agreement (less than 10 %) only limited by the large and increasing background

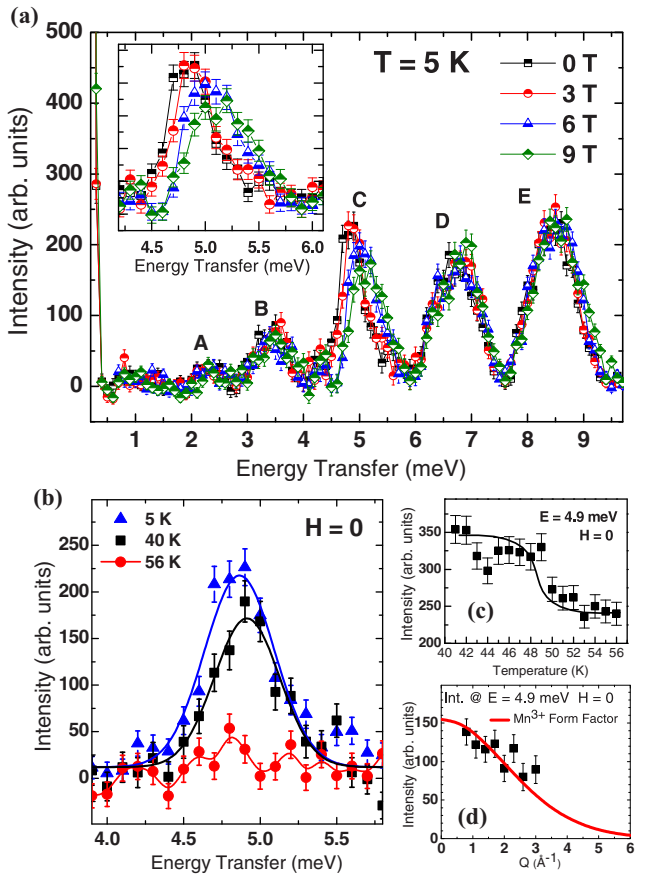

FIG. 5. (Color online) (a) Field-dependence INS spectra in the LS state measured at 5 K under 0–9-T magnetic fields ($k_f = 1.55$ Å^{-1}). Inset: A zoom around the magnetic peak (C) of energy 4.87 meV at zero field. (b) Temperature evolution of magnetic peak (C)[5 and 40 K] at zero field and compared to HS signal at 56 K, with $k_f = 1.55$ Å^{-1}. (c) Peak (C) raw intensity as a function of temperature (40–56 K). (d) Raw intensity as a function of Q of peak (C) at 5 K compared to the Mn^{3+} magnetic form factor squared.

below 0.6 meV. These parameters are successfully used in the calculation of the susceptibility data in the HS state (see Fig. 2) even if some caution is required regarding the g values. The zero-field INS data are in good agreement with the high-field EPR data of Kimura *et al.* [17]: $D = -5.88$ cm^{-1} (0.729 meV) and $E = +0.50$ cm^{-1} (0.062 meV). The parameters obtained from INS could then be used to determine the Landé factors with greater accuracy from single-crystal EPR.

B. Low-spin state $T \leqslant 48$ K

The INS data in the LS state at $Q = 1.35$ Å^{-1} are presented in Fig. 5. First are the INS spectra at 5 K and for four different magnetic field values ($H = 0,3,6,$and 9 T) in the range 0–10 meV [Fig. 5(a)]. Clearly, peak C at 4.87 meV is the only magnetic field dependent peak in this energy range as it shows a shift toward higher energies accompanied by a line broadening. In addition, this is the only peak which disappears on crossing the LS-HS transition as shown in Figs. 5(b) and 5(c). The width of peak C is ≈0.45 meV (twice the elastic resolution) as shown in Fig. 5(b). In addition, we find that the Q dependence of peak C intensity follows, at least in the range $Q = 1$–3 Å^{-1}, the expected Mn^{3+} magnetic form factor [see Fig. 5(d)]. All these observations demonstrate that peak C corresponds to the only magnetic transition observed in the LS state. The magnetization and susceptibility curves (Fig. 2) in the LS state suggest a nonmagnetic ground state with a gap to the first excited state that matches remarkably well the energy suggested by the 4.87-meV (39-cm^{-1}) magnetic peak.

The theoretical description of the LS $^3T_1$ state is more complex than for the ^5E HS state due to the existence of an unquenched first-order orbital moment $L = 1$. A $S = 1$ "spin-only" Hamiltonian model is thus at first sight questionable since the SO coupling must be considered as a first-order perturbation on the $^3T_1$ state. In this framework, it is usual to consider also the effect of an axial ligand field which breaks the degeneracy of the orbital triplet $^3T_1$ term into an orbital singlet ($^3A_2$) and an orbital doublet (^3E). Its effect is introduced by means of a parameter Δ, defined as the separation between the $^3A_2$ and ^3E levels, which is taken to be positive when the orbital singlet lies lowest. These two contributions are commonly treated in the same order in perturbation theory, and the Hamiltonian acting on the $^3T_1$ state then becomes [26]

$$\hat{H}' = \hat{V}_{\rm dis} + \hat{V}_{\rm SO} = \Delta\left(\hat{L}_z^2 - \tfrac{2}{3}\right) - \kappa\lambda\vec{L}\cdot\vec{S}, \qquad (2)$$

where Δ is the uniaxial distortion parameter, $\lambda \approx -180$ cm^{-1} [27] is the many-electron SO coupling constant associated to $^3T_1$, and κ is the orbital reduction factor (close to unity in most cases) which originates from the possible covalency of the metal-ligand bonds. The resulting energy levels, expressed as $(J, \pm M_J)$ [26,28], are represented in Fig. 6 as a function of the uniaxial distortion parameter Δ with $\lambda = -180$ cm^{-1} and $\kappa = 1$. According to this model, the single magnetic transition observed at 4.87 meV between the $(J = 0, M_J = 0)$ ground state and the first excited state necessarily implies that the distortion parameter $|\Delta|$ must be large compared to $\kappa|\lambda|$. Such an energy gap (represented for convenience as arrows in Fig. 6) is achieved for either $\Delta \approx +800$ or -1100 cm^{-1}. A large value of $|\Delta|$ is also consistent with the strong trigonal compression evidenced by diffraction data but its sign remains undetermined since the INS transitions between $\Psi_1(J = 0, M_J = 0)$ and the potential first excited states [$\Psi_2(J = 1, M_J = 0)$ or $\Psi_3(J = 1, M_J = \pm 1)$] are both possible according to neutron selection rules. However, the two cases (positive and negative Δ) lead to radically different magnetic properties.

For large negative Δ, the orbital ground state is the doublet ^3E ($M_L = \pm 1$). Due to SO coupling there are four low-energy levels (see Fig. 6) whose associated states are [in the $\Psi_i(J, M_J)$ notation] $\Psi_1(0,0) = 1/\sqrt{2}(|1,-1\rangle + |-1,1\rangle)$, $\Psi_2(1,0) = 1/\sqrt{2}(|1,-1\rangle - |-1,1\rangle)$, $\Psi_3(1, \pm 1) = |\pm 1,0\rangle$, and $\Psi_4(2, \pm 2) = |\pm 1, \pm 1\rangle$. The energy gap $\delta E_{\Delta<0}$ between the two lowest-lying state Ψ_1 and Ψ_2 is, for large and negative Δ, $\delta E_{\Delta<0} \approx 2(\kappa\lambda)^2/|\Delta|$. In the infinite case ($\Delta/\lambda \gg 1$), Ψ_1 and Ψ_2 converge to the same energy and we are left with three levels characterized by only one quantum number M_J of values $M_J = 0, \pm 1, \pm 2$ and equally separated by $\kappa|\lambda|$ [28]. In this situation, the first magnetic state (Ψ_3, $M_J = \pm 1$) is separated from the ground state Ψ_1 by an energy $\Delta E \geqslant \kappa|\lambda| \approx 180$ cm^{-1}, a value which is too large to explain

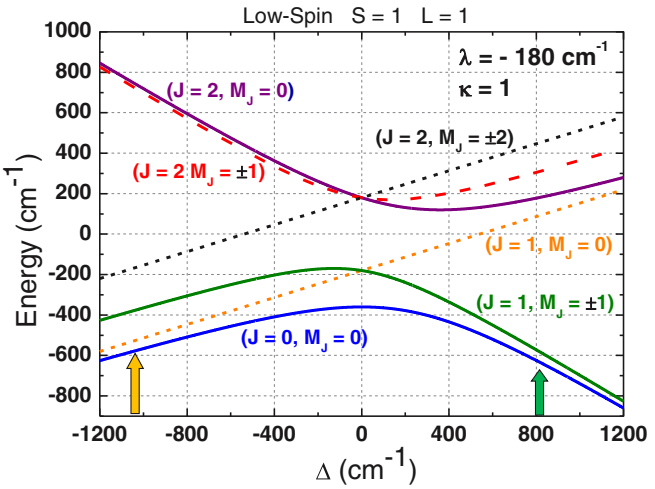

FIG. 6. (Color online) Magnetic states energy diagram in the LS state ($S = 1$, $L = 1$) as a function of the trigonal distortion parameter Δ with orbital reduction factor $\kappa = 1$ and the SO coupling parameter $\lambda = -180$ cm^{-1} (see text for details). The states are labeled in the basis (J, M_J) where $\vec{J} = \vec{L} + \vec{S}$. The three lowest states in energy are, in this basis, $E(0,0) = (1/2)[-(\Delta/3) + \kappa\lambda - \sqrt{(\Delta + \kappa\lambda)^2 + 8(\kappa\lambda)^2}]$, $E(1,0) = (\Delta/3) + \kappa\lambda$, and $E(1, \pm 1) = (1/2)[-(\Delta/3) - \sqrt{\Delta^2 + (2\kappa\lambda)^2}]$. For $\Delta = 0$ the energy spectrum consists of three levels—$E(J = 0) = 2\kappa\lambda$, $E(J = 1) = \kappa\lambda$, and $E(J = 2) = -\kappa\lambda$—whose degeneracy is partially lifted by the axial distortion. Arrows represent the two possible Δ values for which the energy of the first excitation matches the energy of the observed magnetic peak (C) at 4.87 meV (39 cm^{-1}), namely, $\Delta \approx +800$ cm^{-1} in one situation [first excited state equals $E(1, \pm 1)$] or $\Delta \approx -1100$ cm^{-1} in the other situation [first excited state equals $E(1,0)$].

the temperature dependence of the susceptibility in the LS state [see Fig. 2(a)]. Furthermore, Figgis *et al.* showed in the case of a $^3T_1(d^4)$ state that a trigonal compression of the coordination octahedron must lead to a positive value for Δ, rather than a negative value [29,30]. The scenario $\Delta < 0$ is thus very unlikely in this compound.

For large positive Δ, the orbitally nondegenerate $^4A_2$ term ($M_L = 0$) is the lowest and the first-order orbital angular moment is thus quenched. In such a situation the two low-lying energy levels (see Fig. 6) arising from $^4A_2$ upon SO coupling tend to be pure spin states with no orbital contribution: $\Psi(J = 0, M_J = 0) \equiv |0,0\rangle$ and $\Psi(J = 1, M_J = \pm 1) \equiv |0, \pm 1\rangle$ [31]. In this case, a $3d^4$ ion in its LS configuration can be genuinely described by a $S = 1$ spin-Hamiltonian subjected to a ZFS whose associated D term is positive (easy plane) and traduces the energy gap between the ground state $|0,0\rangle$ and the first excited state $|0, \pm 1\rangle$. The Hamiltonian defined in Eq. (1) with $S = 1$ and $E = 0$ (axial case) then applies to this particular case also. This simple spin-only model is found to correctly account for both the susceptibility data ($D \approx 44$ cm^{-1}, *vide supra*) and the observed INS transitions ($D \approx 39.3$ cm^{-1}), strongly supporting the large positive Δ scenario. In this case, the energy gap δE between the two lowest-lying states is given in first approximation by $\delta E_{\Delta>0} \approx (\kappa\lambda)^2/\Delta$ (see Fig. 6). Taking $\kappa \approx 1$, $\lambda \approx -180$ cm^{-1} and considering the experimental gap $\delta E_{\Delta>0} \equiv D = 39.3$ cm^{-1}, we obtain $\Delta \approx +830$ cm^{-1} for $[Mn^{3+}(pyrol)_3(tren)]$ in the LS state.

IV. CONCLUSION

We have reported inelastic neutron scattering (INS), neutron powder diffraction, and magnetometry studies of the thermal spin-transition (ST) mononuclear complex $[Mn^{3+}(pyrol)_3(tren)]$ across the transition temperature $T_{ST} \approx 47$ K. A full spin-Hamiltonian model is proposed in both high-spin (HS) and low-spin (LS) states based on these first INS results obtained in a thermal ST molecular system. In both HS ($S = 2$, $T > T_{ST}$) and LS ($S = 1$, $T < T_{ST}$) states we have determined the microscopic spin and orbital contributions that drive the magnetic properties. In the HS state, the observation of magnetic INS transitions between the zero-field split $S = 2$ ground state enables us to derive the anisotropy parameters ($D = -5.73$ cm^{-1} and $|E| = 0.475$ cm^{-1}) with good accuracy. This result is compatible with a dynamic JT effect that would be spatially averaged over the three N_1-Mn-N_2 distortion directions, thus leading to an effective axial anisotropy direction along the C_3 axis of the molecule. It appears that single-crystal INS could be used advantageously to probe the JT modes individually through phonon spectroscopy, provided large single crystals could be made. In the LS state, the unquenched orbital moment yields a more complex situation where the interplay of spin-orbit coupling and trigonal compression leads to an effective $S = 1$ spin Hamiltonian split by a large positive single-ion anisotropy ($D = +39.3$ cm^{-1}), in good agreement with both INS and susceptibility data. If spectroscopic characterizations of the HS state have been already reported in various Mn^{3+} compounds, the observation and modeling of the $^3T_1$ LS state using a spectroscopic technique like INS have rarely been reported. The strong and positive trigonal ligand-field parameter Δ found in $[Mn^{3+}(pyrol)_3(tren)]$ in its LS state naturally leads to highly anisotropic magnetic properties, but further studies using polarized neutron diffraction will be most helpful to deepen our understanding of this material.

ACKNOWLEDGMENTS

The authors wish to thank G. André, J. Robert, and P. Boutrouille for their support during the neutron-scattering experiments. This work was supported by the Cooperation in Science and Technology (COST) CM1305 program and the FNRS for a postdoctoral scholarship allocated to D.A.S.

[1] J. Linares, E. Codjovi, and Y. Garcia, Sensors **12**, 4479 (2012).
[2] P. Gütlich and H. A. Goodwin, Top. Curr. Chem. **233**, 1 (2004); P. Gütlich, Y. Garcia, and H. A. Goodwin, Chem. Soc. Rev. **29**, 419 (2000); P. Gütlich, A. B. Gaspar, and Y. Garcia, Beilstein J. Org. Chem. **9**, 342 (2013).
[3] M. A. Malcrow, Chem. Soc. Rev. **40**, 4119 (2011).

[4] F. Aguado, F. Rodriguez, and P. Núnez, Phys. Rev. B **76**, 094417 (2007).

[5] Hydrogen bonds may be able to couple at low temperature the magnetic ions through eventual counterions. At high temperature their weakening enables the HS state to set in.

[6] P. G. Sim and E. Sinn, J. Am. Chem. Soc. **103**, 241 (1981).

[7] Y. Garcia, O. Kahn, J. P. Ader, A. Buzdin, Y. Meurdesoif, and M. Guillou, Phys. Lett. A **271**, 145 (2000).

[8] M. Nakano, G. Matsubayahi, and T. Matsuo, Phys. Rev. B **66**, 212412 (2002).

[9] P. Guionneau, M. Marchivie, Y. Garcia, J. A. K. Howard, and D. Chasseau, Phys. Rev. B **72**, 214408 (2005).

[10] Y. Garcia, H. Paulsen, V. Schünemann, A. X. Trautwein, and J. A. Volny, Phys. Chem. Chem. Phys. **9**, 1194 (2007).

[11] P. N. Martinho, B. Gildea, M. M. Harris, T. Lemma, A. D. Naik, H. Müller-Bunz, T. E. Keyes, Y. Garcia, and G. G. Morgan, Angew. Chem. Int. Ed. **51**, 12597 (2012).

[12] G. G. Morgan, K. D. Murnaghan, H. Müller-Bunz, V. McKee, and C. J. Harding, Angew. Chem. Int. Ed. **45**, 7192 (2006).

[13] Z. L. Liu, S. L. Liang, X. W. Di, and J. J. Zhang, Inorg. Chem. Comm. **11**, 783 (2008).

[14] S. Wang, M. Ferbinteanu, C. Marinescu, A. Dobrinescu, Q.-D. Ling, and W. Huang, Inorg. Chem. **49**, 9839 (2010).

[15] K. Pandurangan, B. Gildea, C. Murray, C. J. Harding, H. Müller-Bunz, and G. G. Morgan, Chem. Eur. J. **18**, 2021 (2012).

[16] M. Nakano, G. Matsubayashi, and T. Matsuo, Adv. Quantum Chemistry **44**, 617 (2003).

[17] S. Kimura, T. Otani, Y. Narumi, K. Kindo, M. Nakano, and G. Matsubayashi, J. Magn. Magn. Mater. **272**, 1102 (2004).

[18] S. Kimura, M. Hagiwara, Y. Narumi, M. Nakano, and K. Kindo, J. Phys.: Conf. Ser. **200**, 022025 (2010).

[19] Y. Sawada, S. Kimura, K. Watanabe, and M. Nakano, J. Low. Temp. Phys. **170**, 424 (2013).

[20] P. G. Sim and E. Sinn, Inorg. Chem. **17**, 1288 (1978).

[21] With $N\mu_B^2/(3k_B) = 0.125$ cm^3 K/mol.

[22] B. N. Figgis showed that the magnetic moment reduction compared to its free value due to crystal-field and spin-orbit terms can be expressed as $\mu_{\text{eff}} \approx 2\sqrt{S(S+1)}[1 - 2\lambda/(10Dq)]$ [see B. N. Figgis, Nature (London) **182**, 1569 (1958)].

[23] J. L. Her, Y. H. Matsuda, M. Nakano, Y. Niwa, and Y. Inada, J. Appl. Phys. **111**, 053921 (2012).

[24] S. Bonhommeau *et al.*, Phys. Chem. Chem. Phys. **7**, 2909 (2005).

[25] J. J. Borrás-Almenar, J. M. Clemente-Juan, E. Coronado, and B. S. Tsukerblat, J. Comput. Chem. **22**, 985 (2001).

[26] A. Palii, S. Ostrovsky, S. Klokishner, B. Tsukerblat, C. Berlinguette, K. Dunbar, and J. Galan-Mascaros, J. Am. Chem. Soc. **126**, 16860 (2004).

[27] The negative sign comes from the occupation of the t_{2g} orbitals above half filling in the present case (Mn^{3+}, LS state) [see A. Abragam and B. Bleaney, *Electron Paramagnetic Resonance of Transition Ions* (Oxford University Press, Oxford, 1970)].

[28] B. S. Tsukerblat, A. V. Palii, S. M. Ostrovsky, S. V. Kunitsky, S. I. Klokishner, and K. R. Dunbar, J. Chem. Theory Comput. **1**, 668 (2005).

[29] B. N. Figgis, J. Chem. Soc., 4887 (1965).

[30] B. N. Figgis, J. Lewis, F. E. Mabbs, and G. A. Webb, J. Chem. Soc. A **10**, 1411 (1966).

[31] With $\kappa\lambda = -180$ cm^{-1} and $\Delta = +830$ cm^{-1}, we have in reality expressed in the $|M_L, M_S\rangle$ basis $\Psi(0,0) \approx -0.945|0,0\rangle + 0.231(|1,-1\rangle + |-1,1\rangle)$ and $\Psi(1,\pm 1) \approx \mp 0.979|0,\pm 1\rangle \pm 0.203|\pm 1,0\rangle$.